

Application of the Eckart frame to soft matter: rotation of star polymers under shear flow

Jurij Sablić,¹ Rafael Delgado-Buscalioni,^{2,3, a)} and Matej Praprotnik^{1,4, b)}

¹⁾*Department of Molecular Modeling, National Institute of Chemistry, Hajdrihova 19, SI-1001 Ljubljana, Slovenia*

²⁾*Departamento Física Teórica de la Materia Condensada, Universidad Autónoma de Madrid, Campus de Cantoblanco, E-28049 Madrid, Spain*

³⁾*Condensed Matter Physics Center, IFIMAC, Campus de Cantoblanco, E-28049 Madrid, Spain*

⁴⁾*Department of Physics, Faculty of Mathematics and Physics, University of Ljubljana, Jadranska 19, SI-1000 Ljubljana, Slovenia*

The Eckart co-rotating frame is used to analyze the dynamics of star polymers under shear flow, either in melt or solution and with different types of bonds. This formalism is compared with the standard approach used in many previous studies on polymer dynamics, where an apparent angular velocity ω is obtained from relation between the tensor of inertia and angular momentum. A common mistake is to interpret ω as the molecular rotation frequency, which is only valid for rigid-body rotation. The Eckart frame, originally formulated to analyze the infrared spectra of small molecules, dissects different kinds of displacements: vibrations without angular momentum, pure rotation, and vibrational angular momentum (leading to a Coriolis cross-term). The Eckart frame co-rotates with the molecule with an angular frequency Ω obtained from the Eckart condition for minimal coupling between rotation and vibration. The standard and Eckart approaches are compared with a straight description of the star's dynamics taken from the time autocorrelation of the monomers positions moving around the molecule's center of mass. This is an underdamped oscillatory signal, which can be described by a rotation frequency ω_R and a decorrelation rate Γ . We consistently find that Ω coincides with ω_R , which determines the characteristic tank-treading rotation of the star. By contrast, the apparent angular velocity $\omega < \Omega$ does not discern between pure rotation and molecular vibrations. We believe that the Eckart frame will be useful to unveil the dynamics of semiflexible molecules where rotation and deformations are entangled, including tumbling, tank-treading motions and breathing modes.

PACS numbers: 02.70.Ns, 47.61.-k, 61.20.Ja, 61.25.H-, 83.10.-y, 83.50.-v

^{a)}rafael.delgado@uam.es

^{b)}praprot@cmm.ki.si

I. INTRODUCTION

Soft matter and in particular, polymers, exhibit quite rich dynamics under non-equilibrium conditions. A plethora of collective motions has been described in the literature, not only of polymers, but also of vesicles and more. In a shear flow, the steady state conformation is not possible, and linear polymers perform wild conformational changes stretching and tumbling¹⁻⁶. Star molecules, dendrimers and also vesicles face the shear flow in a different way. They perform internal rotations around the molecule center of mass (CoM), while keeping their overall shape and orientation roughly fixed. This motion has been called tank-treading⁶⁻¹². The case of ring polymers, whose properties have recently been extensively studied^{6,13-15}, is probably in between and recent work indicates that they tumble or tank-tread depending on the value of the shear rate¹⁶⁻¹⁸. Recently, we have observed that star molecules under large enough shear flow perform another collective oscillation, with successive extensions and contractions in their overall length. We called this mode “breathing”¹⁹ and showed that its characteristic frequency Ω_B has the same physical origin as the tumbling frequency in linear and ring chains. The difference being that soft stars do not tumble, but rather let their arms rotate. A similar breathing mode (probably with different mechanical origin) is also observed in vesicles⁷⁻⁹. It could, however, well be that star molecules with attractive inter-monomer interactions (i.e. in bad solvent) would not only tank-tread, but also occasionally tumble (a rotation of the overall molecular shape) like a rugby ball does. One could speculate that the stiffer the intermonomer interactions, the larger the resemblance with a rigid body would be; with some dynamic transition (tank-tread-to-tumble) taking place at moderate attractive energies. Would still those semi-rigid stars breath? These sort of questions on the mechanics of soft deformable macromolecules are difficult to study in clean ways. The reason is clear: at a given time, in the laboratory (inertial) frame, it is not possible to discern between pure rotations and vibrations of the molecule. The simple shear flow is a paradigm of such duality because it is a mix of a pure rotation and a pure shear strain (stretching in one direction and compressing over the perpendicular line). Hybrid affine deformations combining shear and pure elongational flows have also been studied²⁰, enriching the dynamic panorama. The complications of using the laboratory frame to study the rotation of non-rigid molecules have been overlooked in many previous works on polymer dynamics. In particular, a simple estimation of the molecular angular velocity ω based on the polymer shape was first proposed in Ref.²¹. Such relation, stems from the rotation dynamics in the laboratory frame, where the angular velocity ω is related with

the total angular momentum \mathbf{L} and inertia tensor \mathbf{J} as $\mathbf{L} = \mathbf{J} \cdot \boldsymbol{\omega}$. A particularly simple estimations of $\boldsymbol{\omega}$ involving the gyration tensor components, was proposed as rotational-optic rule^{10,21}. Since, many works have reported values of $\boldsymbol{\omega}$ and used it to interpret the polymer rotational dynamics, this has led to erroneous interpretations which is still very much alive in the literature^{10,11,22–25}.

We have recently completed a series of works on star polymer dynamics^{19,26,27}. This series started by a study of the effect of open boundaries compared with closed systems in the rheology of melts under shear (simulations using Open Boundary Molecular Dynamics (OBMD)^{26–28} permits to fix the pressure load and shear stress, instead of the density and shear velocity). As a continuation of such work, we studied the dynamics of stars in solution and melt¹⁹ and observed that the tank-treading frequency of monomers around the molecule’s CoM, ω_R , was completely different from the “apparent” angular velocity obtained from the standard (lab-frame) analysis $\boldsymbol{\omega}$. We also noted that the origin of such strong differences was not explained in previous works. Motivated by these observations, we decided to tackle the problem of soft molecule rotational dynamics using an old and robust formalism, which apparently, has been largely forgotten by the soft matter community: the Eckart co-rotating frame.

The Eckart frame formalism, derived in 1935²⁹, uses a non-inertial frame, which rotates with the molecule. It allows to disentangle translation, rotations, and vibrations. Aside from vibrations without angular momentum contribution (which can be detected in the inertial frame), the non-inertial frame allows to reveal vibrations with angular momentum. These are the displacements with respect to a purely rotating (rigid-body) reference configuration. The Eckart condition determines the rotation frequency of the reference configuration by minimizing the coupling between vibrational angular momentum and pure rotation³⁰. The calculus of the so called “Eckart angular velocity” $\boldsymbol{\Omega}$, can be carried out by the Eckart frame formalism and has been mostly used to study the Raman spectra of small molecules^{31,32} as well as in a variety of other applications, such as structural isomerization dynamics of atomic clusters³³ or molecular dynamics (MD) integration^{34–37}. The “apparent” angular velocity $\boldsymbol{\omega}$ extracted from the total angular momentum in the inertial frame, mixes up pure rotation and vibrational angular momentum. A misinterpretation of this apparent angular velocity had as consequence some large discrepancies in the polymer literature on shear flow^{11,16}.

While the Eckart formalism is traditionally used in equilibrium states, here we use it to describe a situation which is far-away from equilibrium. Although the Eckart condition is first-order accurate, we show that it is robust enough to capture the correct physics. In particular, we show

that the Eckart frame is independent on the reference configuration chosen (see Appendix) and that, for any shear rate, the resulting frequency Ω equals within error bars the monomer rotation frequency about the molecule CoM, ω_R . Star polymers are particularly interesting for this sort of study because of their rich dynamics in shear flow (with tank-treading and breathing modes¹⁹) and also because they represent a bridge between the physics of polymers and colloids^{38–40}. More generally, we expect this work will foster the use of Eckart frame as another useful tool in the analyses of flowing macromolecules' dynamics.

The remainder of the paper is structured as follows: first, we describe the standard (laboratory frame) analysis and the Eckart frame. Then, we describe our working models (star polymer in melt and solution under shear flow). Results and discussion are then presented, followed by conclusions.

II. DYNAMICS DESCRIPTION IN THE LABORATORY FRAME

A standard approach to describe the rotation of molecules is based on the inertial frame (laboratory frame) and follows from a straight generalization of the rigid body rotation, allowing for vibrations without angular momentum contribution $\tilde{\mathbf{v}}$. The kinetic equation for the time evolution of the position of the α monomer \mathbf{r}_α is,

$$\dot{\mathbf{r}}_\alpha = \dot{\mathbf{r}}_{cm} + \boldsymbol{\omega} \times (\mathbf{r}_\alpha - \mathbf{r}_{cm}) + \tilde{\mathbf{v}}_\alpha. \quad (1)$$

In the standard (lab frame) description, the vibrational motion is angular momentum free, and it is denoted by $\tilde{\mathbf{v}}_\alpha$. It is particularly strong in soft molecules as polymers. The corresponding angular frequency is then^{10,11,25}

$$\boldsymbol{\omega} = \mathbf{J}^{-1} \cdot \mathbf{L}. \quad (2)$$

Here, $\mathbf{L} = \sum_{\alpha=1}^N (\mathbf{r}_\alpha - \mathbf{r}_{cm}) \times m_\alpha (\mathbf{v}_\alpha - \mathbf{v}_{cm})$ is the angular momentum of the rotating molecule and \mathbf{J} its moment-of-inertia tensor with respect to the position of its CoM \mathbf{r}_{cm} , defined as

$$\mathbf{J} = \sum_{\alpha=1}^N m_\alpha \{ [(\mathbf{r}_\alpha - \mathbf{r}_{cm}) \cdot (\mathbf{r}_\alpha - \mathbf{r}_{cm})] \mathbf{I} - (\mathbf{r}_\alpha - \mathbf{r}_{cm}) \otimes (\mathbf{r}_\alpha - \mathbf{r}_{cm}) \}, \quad (3)$$

with \mathbf{I} being a 3×3 identity matrix, \mathbf{r}_α the coordinate vector of monomer α of the molecule, and m_α its mass (here $m_\alpha = 1$).

A common mistake is to interpret ω as the molecular angular velocity. However, ω does not describe the pure rotational component of the molecule and in fact, it is called the *apparent angular velocity* in the literature dealing with the Eckart formalism³². Only in the case of rigid-body motion ($\tilde{v} = 0$) does ω coincide with the rotational angular velocity. The reason will come clear in the next section.

III. DESCRIPTION USING THE CO-ROTATING ECKART FRAME

The Eckart formalism permits to dissect yet another kind of vibrations \mathbf{u} , which contribute to the total angular momentum, but *do not contribute to the molecular rotation frequency*. The Eckart frame is a non-inertial frame, which co-rotates with the molecule attached to its CoM. The *pure rotation* frequency Ω is obtained by minimizing the coupling between pure rotation and this vibrational angular momentum: the Coriolis coupling is minimal in this internal moving frame^{29–31}.

The first step of the Eckart frame formalism is to choose some *rigid* molecular configuration, which is taken as the reference one³¹. The Eckart frequency and kinetic energy are, however, independent on the *rigid* reference configuration chosen. This fact is illustrated in the Appendix, where we compare three different reference configurations. Once the reference configuration is chosen, we introduce the initial internal coordinate system, defined by the three right-handed base vectors \mathbf{f}_1 , \mathbf{f}_2 , and \mathbf{f}_3 with the origin in the CoM of the molecule. The initial internal coordinate frame $(\mathbf{f}_1, \mathbf{f}_2, \mathbf{f}_3)$ can be chosen arbitrarily, i.e. its initial orientation is arbitrary. The components of the position vector of the α -th monomer of the reference configuration expressed in the initial internal coordinate system are denoted as c_i^α , $i = 1, 2, 3$. Once defined, the c_i^α s remain constant during the computation of the angular velocity and fulfill the equation^{29,31}:

$$\sum_{\alpha=1}^N m_\alpha c_i^\alpha = 0, \quad \text{for } i = \{1, 2, 3\}. \quad (4)$$

The CoM velocity in thus defined internal coordinate frame is 0 ^{29,31}. From the instantaneous positions of the monomers in the polymer and with the c_i^α s, we define the three Eckart vectors \mathcal{F}_1 , \mathcal{F}_2 , and \mathcal{F}_3 , which are given by^{29,31}:

$$\mathcal{F}_i = \sum_{\alpha=1}^N m_\alpha c_i^\alpha (\mathbf{r}_\alpha - \mathbf{r}_{cm}). \quad (5)$$

From the Eckart vectors, we define a symmetric positive definite Gram matrix \mathcal{F} with the ij -component defined as $[\mathcal{F}]_{ij} = \mathcal{F}_i \cdot \mathcal{F}_j$. The unit base vectors of the instantaneous Eckart frame, (defined by the instantaneous positions of monomers) are computed as^{29,31}:

$$(\mathbf{f}_1, \mathbf{f}_2, \mathbf{f}_3) = (\mathcal{F}_1, \mathcal{F}_2, \mathcal{F}_3) \mathcal{F}^{-1/2}. \quad (6)$$

Here, $\mathcal{F}^{-1/2}$ represents a positively defined matrix, for which the following relation holds:

$$\mathcal{F}^{-1/2} \cdot \mathcal{F}^{-1/2} = \mathcal{F}^{-1}, \quad (7)$$

where \mathcal{F}^{-1} is a positively defined inverse of the Gram matrix \mathcal{F} .

The reference components c_i^α s are in the instantaneous Eckart frame given as:

$$\mathbf{c}_\alpha = \sum_{i=1}^3 c_i^\alpha \mathbf{f}_i. \quad (8)$$

This means that the dynamics of the reference configuration is governed by the time evolution of the positions of the monomers. As mentioned above, the c_i^α s are in general constant and the reference configuration is rigid. Besides, as will be shown below, there is no angular momentum with respect to the internal coordinate system in the zero-th order of displacement of monomers from their reference positions³⁰. Consequently, the dynamics of the reference configuration is nothing but the overall rotation of the molecule, which is described by the angular velocity $\mathbf{\Omega}$.

The rotation of the polymer is defined by the rotation of the base vectors of the Eckart frame:

$$\dot{\mathbf{f}}_i = \mathbf{\Omega} \times \mathbf{f}_i. \quad (9)$$

The combination of Eqs. 8 and 9 yields the following relation³²:

$$\dot{\mathbf{c}}_\alpha = \mathbf{\Omega} \times \mathbf{c}_\alpha. \quad (10)$$

It must be emphasized that there are different ways how to attach the initial internal coordinate system to the reference configuration. Each of these yields different c_i^α s and a different Eckart frame. Nevertheless, once the initial internal coordinate system is chosen, the Eckart frame is defined in a unique way³⁴. The independence on the choice of the *fixed* reference configuration is illustrated in the Appendix, where we report results for three completely different reference configurations: (i) a fixed configuration taken from a frozen $T = 0$ state; (ii) a fixed configuration adapted to the average molecular shape found at each shear rate $\dot{\gamma}$ and (iii) a mobile configuration

which adapts over time to the average molecular conformation upon a pre-determined ‘‘averaging’’ time τ_w . We find that the two fixed configurations give the same Eckart rotation frequency Ω while the third one consistently converges to the outcome of the fixed references for $\tau_w \rightarrow \infty$ while for $\tau_w \rightarrow 0$, it provides the apparent frequency ω obtained from the standard approach.

The reference positions of every monomer in the laboratory frame are computed as:

$$\mathbf{d}_\alpha = \mathbf{r}_{cm} + \mathbf{c}_\alpha, \quad (11)$$

and their instantaneous displacement vectors are defined as

$$\boldsymbol{\rho}_\alpha = \mathbf{r}_\alpha - \mathbf{d}_\alpha. \quad (12)$$

The unit base vectors of the Eckart frame \mathbf{f}_1 , \mathbf{f}_2 , and \mathbf{f}_3 satisfy the Eckart conditions^{29,31}

$$\sum_{\alpha} m_{\alpha} \mathbf{c}_{\alpha} \times \boldsymbol{\rho}_{\alpha} = 0, \quad (13)$$

which state that there is no angular momentum with respect to the internal coordinate system in the zero-th order of displacements of the monomers from their equilibrium positions³⁰. The sketch of the Eckart frame for a star polymer is depicted in Fig. 1.

The angular velocity of the Eckart’s coordinate system is given by:

$$\boldsymbol{\Omega} = \mathbf{J}'^{-1} \cdot \sum_{\alpha=1}^N m_{\alpha} \mathbf{c}_{\alpha} \times (\dot{\mathbf{r}}_{\alpha} - \dot{\mathbf{r}}_{cm}). \quad (14)$$

The tensor \mathbf{J}' is defined as

$$\mathbf{J}' = \sum_{\alpha=1}^N m_{\alpha} \{ [(\mathbf{r}_{\alpha} - \mathbf{r}_{cm}) \cdot \mathbf{c}_{\alpha}] \mathbf{I} - (\mathbf{r}_{\alpha} - \mathbf{r}_{cm}) \otimes \mathbf{c}_{\alpha} \}. \quad (15)$$

In the limit of a rigid molecule, Eq. 15 becomes Eq. 3 and both definitions of angular velocity (given by Eqs. 2 and 14) are equivalent.

The velocity of a given monomer α can be written as^{30,34}:

$$\dot{\mathbf{r}}_{\alpha} = \dot{\mathbf{r}}_{cm} + \boldsymbol{\Omega} \times (\mathbf{r}_{\alpha} - \mathbf{r}_{cm}) + \Delta \mathbf{v}_{\alpha}. \quad (16)$$

The first term on the right hand side of Eq. 16 represents the velocity of molecule’s CoM, the second term is the contribution due to the rotation of the molecule, and the third one, i.e. $\Delta \mathbf{v}_{\alpha}$ due to molecular vibrations. The latter can be expressed as³²:

$$\Delta \mathbf{v}_{\alpha} = \tilde{\mathbf{v}}_{\alpha} + \mathbf{u}_{\alpha}, \quad (17)$$

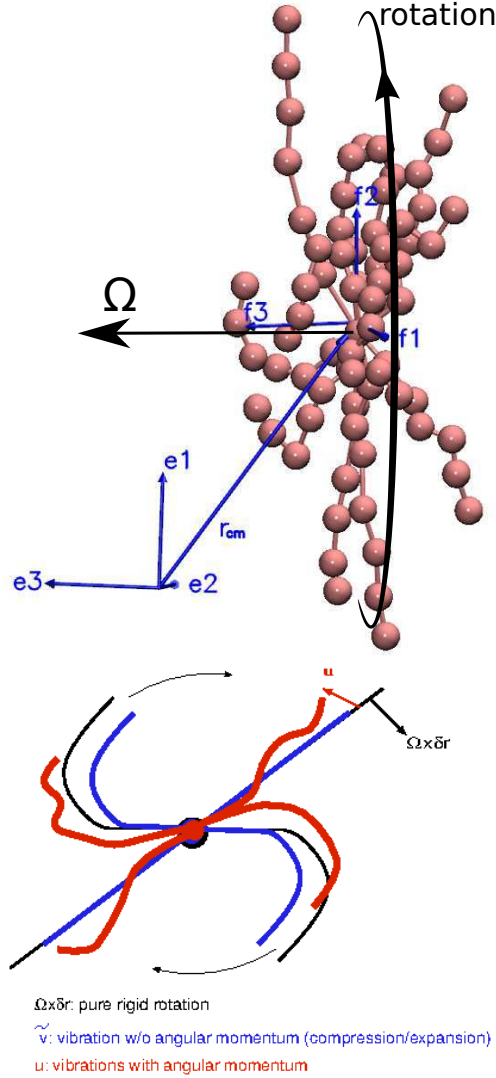


FIG. 1. (Top) A sketch of internal and laboratory frame. The unit base vectors \mathbf{f}_1 , \mathbf{f}_2 , and \mathbf{f}_3 span the internal coordinate system, i.e. the Eckart frame, which translates and rotates together with the molecule. The laboratory frame's base vectors are \mathbf{e}_1 , \mathbf{e}_2 , and \mathbf{e}_3 . The arrows indicate the rotation of the molecule and its vibrations. (Bottom) The sketch gradually introduces the different types of displacements resolved by the Eckart formalism. The black line corresponds to pure rigid rotation (monomer velocity $\Omega \times \delta \mathbf{r}$) which does not introduce molecular deformation. The blue line (velocity $\tilde{\mathbf{v}}$) introduces vibrations without angular momentum contribution (e.g. compression and expansion) and the red line introduces vibrations with angular momentum (fluctuations with velocity \mathbf{u}) which deform the molecule's shape (e.g. due to Brownian diffusion). Note that $\mathbf{u} \cdot \Omega \times \delta \mathbf{r} < 0$ (Coriolis term). The different velocities are explained in the text (see e.g. Eqs. 16 and 17).

where \mathbf{u}_α represents the angular motion part and $\tilde{\mathbf{v}}_\alpha$ (the same as in Eq. 1) the angular motion free part of the vibrational motion. Comparing the expressions in Eqs. 1 and 16, one derives the following equation³²:

$$\mathbf{u}_\alpha = (\boldsymbol{\omega} - \boldsymbol{\Omega}) \times \delta \mathbf{r}_\alpha, \quad (18)$$

with $\delta \mathbf{r}_\alpha \equiv \mathbf{r}_\alpha - \mathbf{r}_{cm}$. This means that \mathbf{u}_α is the part of α -th monomer's vibrational motion, which is coupled with rotations if the angular velocity is calculated by the standard approach. It can be decoupled from rotations by using the Eckart frame formalism.

According to Eq. 1, the kinetic energy $T = \frac{1}{2} \sum_\alpha m_\alpha \dot{\mathbf{r}}_\alpha^2$ of any rotating molecule can be written as:

$$T = \frac{1}{2} M \dot{\mathbf{r}}_{cm}^2 + \frac{1}{2} \boldsymbol{\omega} \cdot \mathbf{J} \cdot \boldsymbol{\omega} + \frac{1}{2} \sum_\alpha m_\alpha \tilde{\mathbf{v}}_\alpha^2, \quad (19)$$

where $M = \sum_\alpha m_\alpha$ the molecule's mass. These three terms in the right hand side, are collected into,

$$T = T_{trans} + T_{rot}^{lab} + T_{vib}^{lab}, \quad (20)$$

with T_{trans} , T_{rot}^{lab} , and T_{vib}^{lab} the translational, rotational, and vibrational contributions to the kinetic energy.

On the other hand, using the Eckart frame, the velocity of each monomer is expressed by Eq. 16 and the kinetic energy of a molecule is decomposed as³²

$$T = \frac{1}{2} M \dot{\mathbf{r}}_{cm}^2 + \frac{1}{2} \boldsymbol{\Omega} \cdot \mathbf{J} \cdot \boldsymbol{\Omega} + \frac{1}{2} \sum_\alpha m_\alpha \tilde{\mathbf{v}}_\alpha^2 + \frac{1}{2} \sum_\alpha m_\alpha \mathbf{u}_\alpha^2 + \sum_\alpha \mathbf{u}_\alpha \cdot (\boldsymbol{\Omega} \times \delta \mathbf{r}_\alpha). \quad (21)$$

One can now distinguish the following terms (in order of appearance in the RHS of Eq. 21):

$$T = T_{trans} + T_{rot}^{Eck} + T_{vib-non-ang}^{Eck} + T_{vib-ang}^{Eck} + T_{Cori}^{Eck}. \quad (22)$$

Here, T_{rot}^{Eck} denotes pure rotational contribution. The vibrational contribution consists of two parts: the first, emerging from the angular free part of the vibrational motion, is denoted by $T_{vib-non-ang}^{Eck}$, and the second, i.e. $T_{vib-ang}^{Eck}$, representing the angular part of vibrations. The last contribution is the Coriolis coupling, which is denoted by T_{Cori}^{Eck} . Comparing both kinetic energy expressions (i.e. in Eqs. 19 and 21), we observe that the following relations hold

$$T_{vib}^{lab} = T_{vib-non-ang}^{Eck}, \quad (23)$$

$$T_{rot}^{lab} = T_{rot}^{Eck} + T_{vib-ang}^{Eck} + T_{Cori}^{Eck}. \quad (24)$$

TABLE I. The different frequencies mentioned in this work.

ω	Apparent angular velocity	Eq. 2
Ω	Eckart angular velocity	Eq. 14
ω_R	Monomer rotation frequency	Eq. 28
Ω_B	Breathing mode frequency	From Eq. 30

and obviously, the translational kinetic energy T_{trans} is the same in both frames. In order to alleviate the notation, we define the pure rotational energy T_{rot}^{Eck} , the angular-momentum free vibrational energy $T_{\tilde{v}}$, and the net vibrational angular momentum energy T_u as,

$$T_{\Omega} \equiv \frac{1}{2} \Omega \cdot \mathbf{J} \cdot \Omega = T_{rot}^{Eck}, \quad (25)$$

$$T_{\tilde{v}} \equiv \frac{1}{2} \sum_{\alpha} m_{\alpha} \tilde{\mathbf{v}}_{\alpha}^2 = T_{vib}^{lab} = T_{vib-non-ang}^{Eck}, \quad (26)$$

$$T_u \equiv \frac{1}{2} \sum_{\alpha} m_{\alpha} \mathbf{u}_{\alpha}^2 + \sum_{\alpha} \mathbf{u}_{\alpha} \cdot (\Omega \times \delta \mathbf{r}_{\alpha}) = T_{vib-ang}^{Eck} + T_{Cori}^{Eck}. \quad (27)$$

In the next section, we resort to the Eckart frame formalism in the analysis of the rotational and vibrational behavior of star polymers in solution and melt. Differences with respect the laboratory frame will be highlighted.

IV. RESULTS AND DISCUSSION

In this section, we present results from two different types of systems: i) a single star polymer in solution (representing a dilute polymer suspension) and ii) a melt of star polymers, with polymer volume fraction $\phi = 0.2$ under isothermal conditions. The molecular model of the star polymer is the same in both types of simulations. In the solution case, we consider two types of bonds between monomers (blobs): harmonic bonds and finitely extensible non-linear elastic (FENE) bonds. In melt simulations, we use harmonic bonds to build up the star molecule.

We have so far introduced two frequencies (i.e. ω and Ω) describing rotation in polymers. In what follows, we will introduce two additional frequencies and for the sake of clarity and reference, we list them all in Table I.

To present the results in non-dimensionalized form, we use the Weissenberg numbers Wi and Wi_{rot} . The latter is based on rotational diffusion time of the star. This is defined as $Wi_{rot} = \dot{\gamma} \tau_{rot}$ where τ_{rot} is the time for rotational diffusion $\tau_{rot} = R^2/D_r$ of the molecule in equilibrium (see^{19,27}

TABLE II. The rotational diffusion and arm-disentanglement relaxation times for our star model, with 12 arms and 6 monomers per arm. We define $Wi_{rot} = \dot{\gamma}\tau_{rot}$ and $Wi = \dot{\gamma}\tau_{rel}$ with $\tau_{rel} = \max[\tau_{rot}, \tau_{dis}]$.

System	τ_{rot}	τ_{dis}
closed melt: $\gamma_{\parallel} = 1.0, \gamma_{\perp} = 1.0$	710 ± 40	390 ± 10
open melt: $\gamma_{\parallel} = 1.0, \gamma_{\perp} = 1.0$	700 ± 40	390 ± 10
solution harmonic bonds	270 ± 20	180 ± 20
solution FENE bonds	370 ± 30	950 ± 90

for details). The Wi , on the other hand, is based on the largest relaxation time (τ_{rel}) of the molecule, i.e. $Wi = \dot{\gamma}\tau_{rel}$. It has to be said that the molecular rotational diffusion is the slowest relaxation process for stars with harmonic bonds, while for star molecules with FENE bonds, the slowest relaxation is the process of arm disentanglement. The corresponding relaxation times (rotational and arm-disentanglement) for simulations in solution and in melt are given in Table II.

A. Star polymer models

The star polymer model is taken from Ref.⁴¹. We use the standard Lennard-Jones units, taking the monomer mass m_0 , unit length σ_0 and energy ϵ_0 as reference. We consider stars with $f = 12$ arms and $m = 6$ beads per arm, with a total of 73 monomers (including the central one). Excluded volume interactions of monomers are modeled by the repulsive Weeks-Chandler-Anderson interaction ($\sigma = 2.415$ and $\epsilon = 1$). The bonds between adjacent monomers i and j are modelled by either harmonic springs or FENE bonds. In the case of harmonic bonds, with a recovery force $-K(r_{ij} - r_{ij}^{eq})$, the spring constant is $K = 20$ and the equilibrium distance $r_{ij}^{eq} = 2.77$ (the equilibrium distance between the central monomer and the first monomer of an arm is larger $r_{ij}^{eq} = 3.9$). Finitely extensible bonds are modeled by the FENE potential⁴², with a spring constant $K = 20$ and maximum length of the bond $r_{max} = 1.5 r_{ij}^{eq}$.

B. Melt simulations

For the melt case, we use stars made of harmonic bonds. Simulations are carried out at fixed temperature $T = 4$ using molecular dynamics with a dissipative particle dynamic (DPD) thermostat^{43,44}. We solve systems with constant volume (closed setup) and also open systems un-

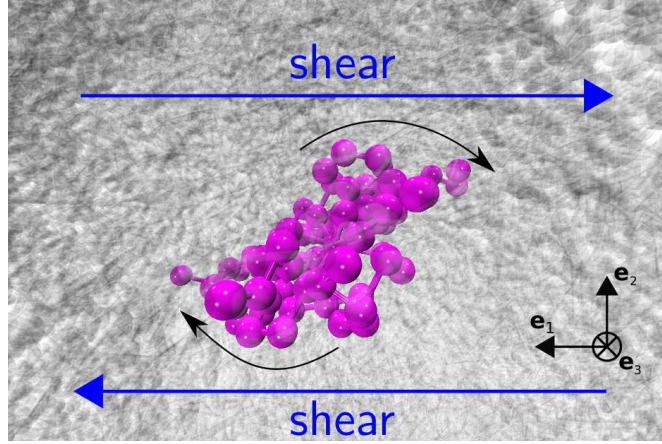


FIG. 2. Snapshot of the star-polymer melt under shear flow, drawn from the perspective of one polymer. The latter is depicted in purple and its surrounding polymers are colored in gray. The blue arrows correspond to the direction of the imposed shear, while the black arrows indicate the tank-treading rotation of the polymer. The coordinate unit vectors \mathbf{e}_1 , \mathbf{e}_2 , and \mathbf{e}_3 define the flow (x_1), the gradient (x_2), and the neutral (x_3) direction, respectively.

der constant normal load (see Ref. for details²⁷). The simulation box is of size $390 \times 117 \times 117$ and the density of the melt in equilibrium corresponds to the occupational factor $\Phi = 0.2$, with about 2000 molecules. In the closed periodic setup, the shear flow is imposed by the SLLOD algorithm implemented with the Lees-Edwards boundary conditions⁴⁵⁻⁴⁷. Constant load simulations in an open system, are performed using OBMD^{26,28,48,49}, which permits to impose an external shear stress at the open ends of the system. We shall use the following coordinates: x_1 refers to the flow direction, x_2 to the direction of the velocity gradient and x_3 to the direction of flow vorticity (sometimes called neutral direction). The DPD thermostat used here introduces friction along the *normal* and *tangential* directions of any pair of monomers^{27,41,43,44} which come closer than the DPD-cutoff radius $R_{DPD} = 2 \times 2^{1/6} \sigma$ (we use a Heaviside kernel for the DPD interaction). The friction coefficients in normal and tangential directions equal $\gamma_{\parallel} = 1.0$ and $\gamma_{\perp} = 1.0$. The equations of motion are integrated by the Velocity-Verlet algorithm⁵⁰ with the integration step 0.01τ for small and moderate shear, and 0.005τ for high shear rates. A sketch of the star-polymer melt under shear flow from the perspective of one of its constituent polymers is depicted in Fig. 2.

C. Star in solution

We simulate a single star polymer in solution using Brownian hydrodynamics^{51,52}. The monomers (representing a coarse description of the molecule) interact via conservative forces (bonds and excluded volume interactions) and also via hydrodynamic interactions. The displacement of monomer α in direction i over time dt has the form $dr_i^\alpha = \dot{\gamma}x_2^\alpha\delta^{i,1}dt + \mu_{ij}^{\alpha\beta}(r_{\alpha\beta})F_j^\beta dt + d\tilde{r}_i^\alpha$ where the first term indicates the shear flow (acting in 1-direction) and the mutual drag arises from the mobility tensor $\mu_{ij}^{\alpha\beta}$ which in present calculations consists on the Rotne-Prager-Yamakawa (RPY) approximation^{51,52}. The Brownian displacement $d\tilde{\mathbf{r}}$ satisfies a fluctuating dissipation (FD) relation for its covariance $\langle d\tilde{r}_i^\alpha d\tilde{r}_j^\beta \rangle = 2k_B T \mu_{ij}^{\alpha\beta} dt$ and to solve $d\tilde{\mathbf{r}}$ we use the Fixman's method⁵². The integration scheme is an explicit Euler scheme with the time step $dt = 0.01\tau$. In the present study, all simulations are run for 10000τ .

D. Monomer rotation dynamics

To provide direct connection with the monomer dynamics, we calculate the angular velocity of rotation of molecules from the autocorrelation function of the gradient-direction coordinate of the last monomer of every arm of the star, relative to the CoM, $(\mathbf{r}_\alpha - \mathbf{r}_{cm}) \cdot \hat{\mathbf{x}}_2$. This signal is similar to an underdamped oscillator (Fig. 3) which can be fitted with the following function⁵³:

$$C(t) = A^2 \cos(\omega_R t + \psi) \exp(-\Gamma t), \quad (28)$$

where the damping rate Γ represents the decorrelation rate, ω_R the rotation frequency, and ψ a phase constant. Two issues are noticeable from this graph: first, the decorrelation rate Γ only starts to significantly increase above $Wi_{rot} > 50$. Second, as Wi increases, the quality factor $q = \omega_R/\Gamma$ becomes quite large, in particular, compared with what happens in linear polymers under shear⁵³ (which tumble by compressing, like in a tube). Figure 3 (bottom panel) compares the quality factor q for star polymers in solution (S) and melt (M) (with either FENE or harmonic bonds) and that measured in Ref.⁵³ for FENE linear chains with $N = 60$ and dumbbells. In the case of star molecules, the arms rotate almost like in a “wheel” and a monomer turns around several times (q) before decorrelating its initial “rigid-body” position. At large shear rates, the differences in values of q are significant [see Fig. 3 (bottom)]. The quality factor is significantly smaller in melts, indicating the hindrance arising from steric interaction amongst close-by molecules. In

TABLE III. Kinetic energy balance for solution of star polymers with harmonic and FENE bonds. The error bar of the reported values is approximately 5%.

solution harmonic bonds					solution FENE bonds				
W_i	T	T_Ω	$T_{\bar{v}}$	T_u	W_i	T	T_Ω	$T_{\bar{v}}$	T_u
13.25	1102	412	1028	-338	9.5	875	303	794	-222
53	1117	517	1042	-442	95	876	365	793	-282
106	1135	464	1058	-387	570	912	498	808	-394
424	1363	1189	1275	-1101	1520	1086	763	919	-596

what follows, we will compare ω_R with ω and Ω and discuss the origin of the decorrelation Γ , according to the Eckart analysis.

E. Kinetic energies

The kinetic energy balance is illustrated in Table III for star molecules in solution (having harmonic or FENE bonds) and some values of the shear rate. Displacements describing pure rotations have kinetic energy T_Ω but, coherent (collective) vibrations without angular momentum contribute with the largest energy $T_{\bar{v}}$. These are related to overall shape deformations (and in particular, compression/expansion does not introduce angular momentum). Other type of molecular deformations (affine or not) are collected in the velocity \mathbf{u}_α which does provide angular momentum (see Eq. 18) and feeds the (negative) kinetic energy contribution $T_u = T_{vib-non-ang} + T_{Cori}$ (see Table III and Eq. 23). Equation 27 confirms that this energy can only be negative because of the Coriolis term. So, in average, $\mathbf{u} \cdot (\Omega \times \delta\mathbf{r}) < 0$; in other words \mathbf{u} contributes in opposite direction to the pure rotation velocity $\Omega \times \delta\mathbf{r}$. Note that $|T_u|$ is subtracted to the pure rotation energy T_Ω to yield the total rotation kinetic energy in the lab frame T_{rot}^{lab} (see Eq. 24). To clarify matters, a sketch illustrating the different types of displacements is drawn in Fig. 1 (bottom panel). In what follows, we analyze these kinetic energies separately.

F. Pure rotation: tank-treading

Figure 4 compares the results for the apparent angular velocity ω , the Eckart angular velocity Ω and the frequency of monomers rotation about the CoM ω_R . In all considered cases (polymers

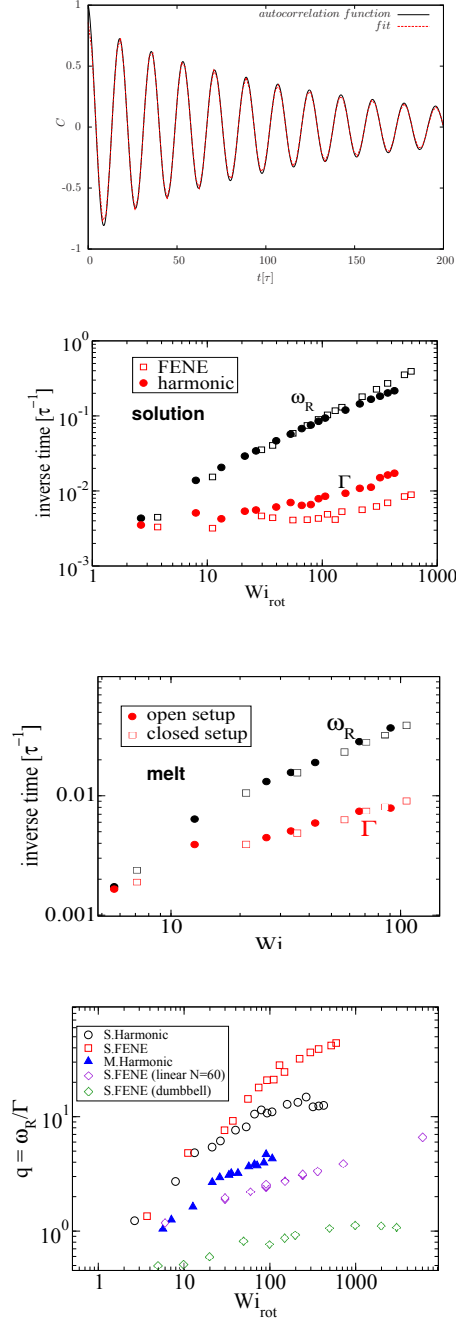


FIG. 3. (Top) Autocorrelation function of position of the final monomers of each polymer's arm in the gradient direction, fitted by Eq. 28 with parameters: $A = 0.93$, $\omega_R = 0.35$, $\Gamma = 0.0084$, and $\Psi = 0.0025$. (Middle panels) The tank-treading frequency ω_R and decorrelation rate Γ obtained from the fits (stars in solution and in melt). (Bottom) The quality factor $q = \omega_R/\Gamma$ for the dynamics of monomer rotations, comparing our 12-6 stars with linear FENE chains ($N = 60$) (with excluded volume interactions) and dumbbells, from Ref.⁵³.

with either harmonic or FENE bonds in solution, and the melt case), we find that $\Omega = \omega_R$ within error bars while $\Omega > \omega$. Whenever vibrational angular momentum is present, the apparent angular velocity ω does not correctly represent molecular rotation³². The difference between ω and Ω is larger for stars with Hookean-bonds in solution (see Fig. 4). From Eq. 18, this simply indicates that vibrational angular momentum (\mathbf{u}_α) has a larger contribution if the molecule is softer (harmonic versus FENE bonds) or has more free space to deform (as in the case of solution compared to melt).

Stars with harmonic bonds in solution seems to reach the scaling $\omega/\dot{\gamma} \sim \text{Wi}^{-1}$ (i.e. $\omega \rightarrow \text{cte}$) as the shear rate is increased (although, in fact, at very large $\dot{\gamma}$, ω decreases). This apparent scaling was attributed in Ref.¹¹ (and subsequent citations) to an universal limiting trend for tank-treading rotation of star polymers. However, although the apparent angular velocity ω reaches a maximum value, the tank-treading frequency ω_R , keeps increasing with $\dot{\gamma}$, like $\omega_R \sim \text{Wi}^\alpha$ with $\alpha = 0.5 \pm 0.02$. This is shown in Fig. 4) where one can see that ω and ω_R differ significantly.

Finally, in melts, (bottom panel of Fig. 4) we observe that the molecular rotational frequencies are similar in the open and closed environments. This is in agreement with our previous studies (Ref.^{19,27}) and indicates that the rheological differences measured in open and closed environments are of thermodynamic origin (density decreases when an open polymer enclosure is sheared).

G. Vibrational angular momentum and decoherence of rotational motion

Following this line, Eq. 24 indicates that the total kinetic energy coming from displacements with angular momentum can be decomposed in a pure rotational part T_Ω and contributions from vibrational angular momentum. It is noted that T_Ω contains contributions from collective displacements and also from fluctuations. Equation 25 indicates that

$$T_\Omega = \frac{N}{2} \Omega_3^2 (G_{11} + G_{22}) + \tilde{T}_{rot}, \quad (29)$$

where \tilde{T}_{rot} introduces a significant contribution from the covariances involving zero-average components of the rotational frequency Ω , like $\tilde{T}_{rot} = \langle N \Omega_1^2 G_{22} \rangle + \dots$. Here, G_{ii} represents the diagonal gyration tensor component in the i -th direction.

The energy of vibrations with angular momentum corresponds to deformations of the arms away from pure rigid body rotation (see Eq. 18). In solution, these motions arise from Brownian diffusion so we expect that the kinetic energy $|T_u|$ is proportional to ΓD_{arm} where D_{arm} is the

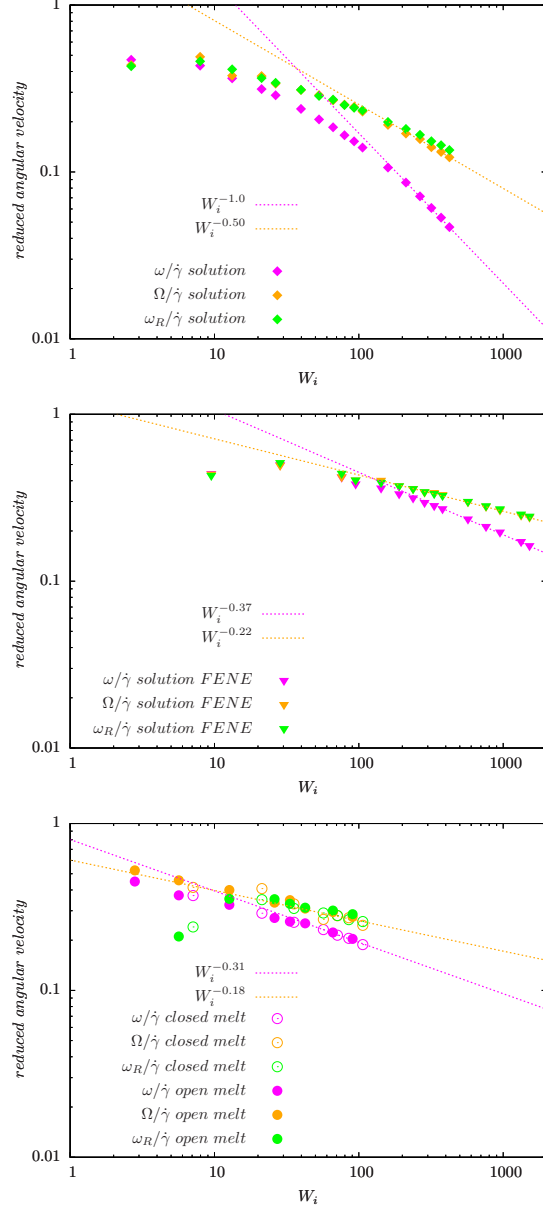


FIG. 4. Comparison of the angular velocity computation by the Eckart frame formalism ($\Omega/\dot{\gamma}$ - colored in orange), by the standard approach ($\omega/\dot{\gamma}$ - colored in magenta), and by the autocorrelation function of the position of the final monomers in every polymer's arm in the gradient direction ($\omega_R/\dot{\gamma}$ - colored in green). We study rotations in the solution of star polymers with Hookean (Top) and FENE bonds (Middle) and in the melt of star polymers with Hookean springs (Bottom). In all three systems, the angular velocity obtained by the Eckart frame formalism is higher than the one calculated by the standard approach. In all cases, ω_R matches well with Ω while the difference $\omega - \omega_R$ is larger in the Hookean spring solution case, followed by the solution of molecules with the FENE bonds and the melt. The reasons for these facts are explained in the text.

diffusion coefficient of the center of mass of one star’s arm (which is independent on the shear rate). The scaling this hypothesis predicts is validated in Fig. 5 where $|T_u|$ (normalized with its value at zero shear rate) is compared with $\Gamma\tau_{rot}$ for increasing Weissenberg number. Results for different types of star polymers (harmonic and FENE bonds) confirm that both magnitudes are proportional and indicate that our intuition contains physical insight. In melts, however, both quantities differ significantly (see Fig. 5 bottom panel) indicating that, in this case, molecular deformations are also determined by other (non-Brownian) mechanisms, like inter-molecular collisions.

H. Vibrations without angular momentum and breathing mode

As stated (see Table III), vibrations without angular momentum $T_{\bar{v}}$ have the largest contribution to the kinetic energy of the star molecule. This kinetic energy has also a thermal and a coherent contribution. The thermal energy includes the fluctuations in bond length, whose average kinetic energy scales like $N_{sp}K\langle\delta^2\rangle$, with $\delta = r_{\alpha,\beta} - r_{eq}$ the bond length, $N_{sp} = 72$ the number of springs in our star molecules and K their spring constant. Excluded volume forces are also central forces $\mathbf{F}_{\alpha,\beta} \propto \hat{\mathbf{r}}_{\alpha,\beta}$ ($\hat{\mathbf{r}}_{\alpha,\beta}$ being the unit distance vector between monomers α and β) so in absence of hydrodynamic interactions they strictly do not contribute to the total angular momentum. It is noted that hydrodynamics spreads over internal forces, and contributes to the angular momentum, with monomer displacements $d\mathbf{r}_\alpha = \boldsymbol{\mu}_{\alpha\beta}\mathbf{F}_\beta dt$, where $\boldsymbol{\mu}_{\alpha\beta}$ is the mobility tensor. However, as shown in Ref.¹⁹, the major source of angular momentum comes out from the mean flow. We assume that thermal contribution to $T_{\bar{v}}$ is independent on the shear rate. The remaining contribution to $T_{\bar{v}}$ is assumed to be associated to overall deformations of the molecular shape and should increase with $\dot{\gamma}$. This separation between thermal and coherent vibrations is clearly revealed in the fit $T_{\bar{v}}(\text{Wi}) = T_{\bar{v}}(0) + \Delta T_{\bar{v}}(\text{Wi})$, which is shown in Fig. 6, with $T_{\bar{v}}(0) = 1029 \pm 5$ and $\Delta T_{\bar{v}}(\text{Wi}) = 0.021 \text{Wi}^{1.54}$ for harmonic springs and while $T_{\bar{v}}(0) = 792 \pm 2$ and $\Delta T_{\bar{v}}(\text{Wi}) = 2.32 \times 10^{-5} \text{Wi}^{2.12}$ for FENE bonds (both in solution). In the case of melts we find $T_{\bar{v}}(0) = 426$ and $\Delta T_{\bar{v}}(\text{Wi}) = 4.60 \times 10^{-4} \text{Wi}^{2.00}$.

We expect that the coherent part of the vibrational energy $\Delta T_{\bar{v}}(\text{Wi})$ comes out from a collective “oscillation” of the molecule shape. Such type of collective vibration was discussed in a previous work on star polymers¹⁹, and was referred to as “breathing mode”. The dynamics of the breathing mode is revealed in the time correlation of the components of the gyration tensor (G_{ij}), given

by^{3,16,19},

$$C_{ij}(t) = \frac{\langle \delta G_{ii}(t_0) \delta G_{jj}(t_0 + t) \rangle}{\sqrt{\langle \delta G_{ii}^j(t_0) \rangle \langle \delta G_{jj}^2(t_0) \rangle}}. \quad (30)$$

where $\delta G_{ii} = G_{ii} - \langle G_{ii} \rangle$. These are damped oscillatory signals with a characteristic frequency Ω_B . In previous works^{16,19}, the cross-correlation C_{12} has been used to extract the ‘‘tumbling’’ time τ_t (as twice the difference between first maximum and first minimum). We define $\Omega_B = 2\pi/\tau_t$. As explained in Ref.¹⁹, these type of dynamics have been called ‘‘tumbling’’ in linear and ring chains, while the word ‘‘breathing’’ is more appropriate to describe the star overall shape oscillation, while they perform tank-treading. The energy of ‘‘breathing’’ can be estimated from the largest fluctuation in the gyration tensor, taken from the standard deviation of the principal eigenvalue of the gyration tensor \mathbf{G} , i.e. $\text{Std}[G_1] = \langle (G_1 - \langle G_1 \rangle)^2 \rangle^{1/2}$. A rough estimation of the breathing kinetic energy is then, $T_B \equiv \frac{N}{2} \Omega_B^2 \text{Std}[G_1]$, and it is compared with $\Delta T_{\bar{v}}$ in Fig. 6. In passing, we note that a quite similar outcome is obtained by $T_B \propto \Omega_B^2 \text{Std}[V^{2/3}]$ which is based on fluctuations (expansion/contraction) of the overall molecular volume $V = \prod_{\alpha} G_{\alpha\alpha}^{1/2}$. Interestingly, we find an excellent agreement (even quantitative) in all cases involving stars with harmonic bonds (solution and melt). However, in the FENE case, the values of T_B and $\Delta T_{\bar{v}}$ differ at small and moderate shear rate, and become similar as Wi increases. For moderate and small Wi we find $\Delta T_{\bar{v}} < T_B$, indicating that the stronger excluded volume forces in FENE bonds (arm elongations are confined to a fixed value) tend to reduce collective vibrations (breathing) of the star molecules.

I. Intrinsic viscosity

One of the major tasks of polymer physics is to relate individual chain dynamics with macroscopic rheological properties. We make such an exercise in this section, taking the shear viscosity as our target macroscopic quantity. In a previous work, we analyzed in some detail the rheology of these stars in melt¹⁹ and reported in particular its shear viscosity under shear. Here, we calculate the contribution to the shear viscosity of star polymers in solution from their contribution to the virial part of the shear stress tensor⁵⁴,

$$\boldsymbol{\sigma} = \rho_P \left\langle \sum_{\alpha=1}^N (\mathbf{F}_{\alpha}^{nb} + \mathbf{F}_{\alpha}^b) \otimes (\mathbf{r}_{\alpha} - \mathbf{r}_{cm}) \right\rangle. \quad (31)$$

Here, \mathbf{F}_{α}^{nb} represents the force on the α -th monomer, originating from the non-bonded interactions (i.e. the Weeks-Chandler-Anderson interaction), and \mathbf{F}_{α}^b are the forces of the bonds (i.e. either

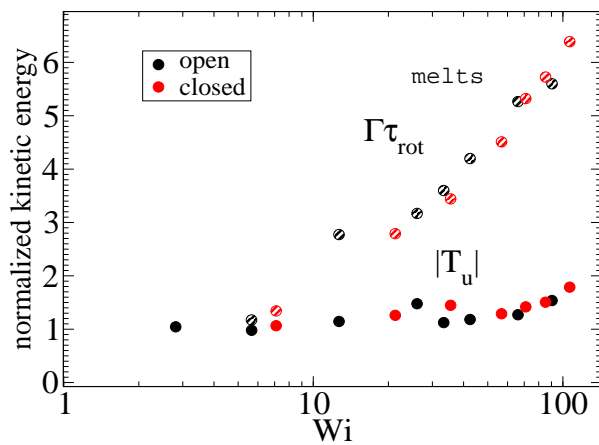
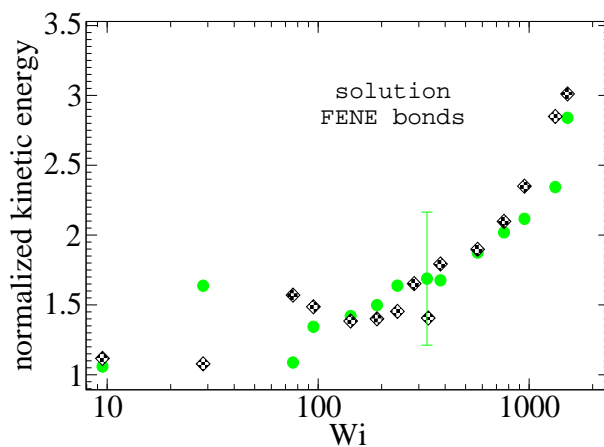
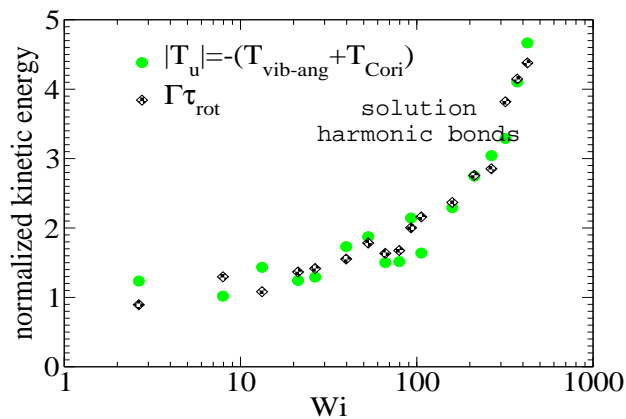


FIG. 5. The absolute value of kinetic energy related to vibrational non-angular momentum $|T_u|$ compared with the rate of decorrelation (Γ) of the monomer pure rotation around the molecule center (see Fig. 3). Both quantities are normalized with their values at zero shear rate. Top and middle panel, results for solution and bottom panel, for the melt.

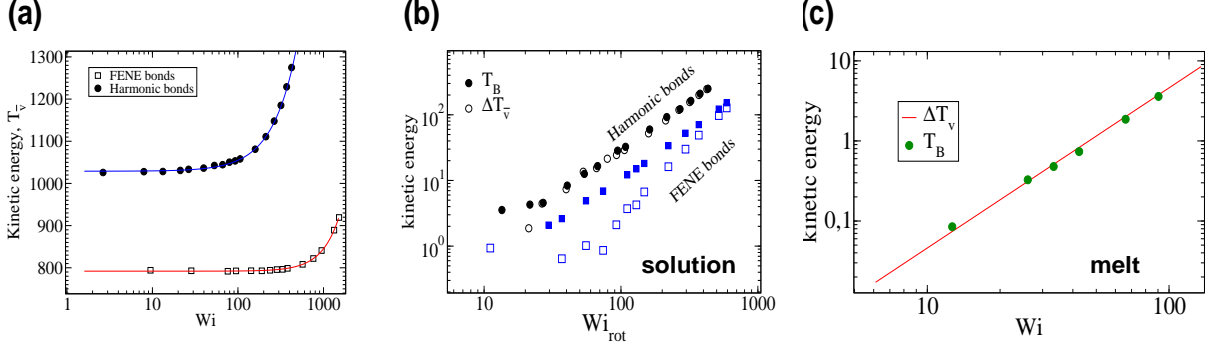


FIG. 6. (a) The angular momentum free vibrational kinetic $T_{\bar{v}}$ (symbols) and the fit $T_{\bar{v}}(Wi) = T_{\bar{v}}(0) + aWi^{\beta}$ with $\Delta T_{\bar{v}} = aWi^{\beta}$ the coherent part and $T_{\bar{v}}(0)$ the thermal contribution (results for star in solution). (b) The coherent contribution $\Delta T_{\bar{v}}$ is compared with the breathing mode energy estimated as $T_B = \frac{N}{2}\Omega_B^2 \text{Std}[G_1]$, where G_1 is the principal eigenvalue of the gyration tensor and Ω_B is the breathing frequency, reported in Ref.¹⁹ (results for solution). (c) The same as (b) but for the melt case, and $T_B = 0.45 \frac{N}{2}\Omega_B^2 \text{Std}[G_1]$.

harmonic or FENE). The polymer contribution to the stress tensor is proportional to ρ_P , the number density of polymer molecules, and the polymer contribution to the shear viscosity is⁵⁴

$$\eta = -\frac{\sigma_{12}}{\dot{\gamma}}. \quad (32)$$

Using the Carreau fit^{55,56}, we estimate the zero-shear rate viscosity η_0 and present the normalized viscosity η/η_0 . We note that η_0 is about 1.8 times larger in the case of the harmonic-bond model compared with the FENE bonds. As the shear rate is increased, we find shear thinning $\eta \sim Wi^{-\beta}$ with shear thinning exponents $\beta = 0.25$ for FENE bonds and $\beta = 0.32$ for harmonic bonds. These values are somewhat smaller than those found in melt, $\beta = 0.49$ (see Fig.7). Viscous dissipation is related to decorrelation times and in fact, the intrinsic viscosity can be expressed as an sum of relaxation times⁵⁷. For an isolated star in dilute solution, one expects that the main mechanism for dissipation comes from the decorrelation in arm lengths, which takes place at an average rate Γ (see Fig. 3). Thus, as a first estimate, we seek a relation of the form $\eta \propto \Gamma^{-1}$. Figure 7 shows that such relation holds relatively well, both in solution and melts. For instance, in solution we see that the softer harmonic bonds leads to faster decorrelation rates and smaller intrinsic viscosity, compared with the more rigid FENE chains. As we indicated in Fig. 5, we found that, in solution, Γ scales like the kinetic energy $|T_u|$ and consistently, $|T_u|$ is larger in the case of harmonic bonds compared with FENE-stars. In melts, however, one expects that the departure from rigid-body rotation (measured by the velocity u and its kinetic energy T_u) arises also from inter-molecular collisions (and not only from Brownian diffusion). This is revealed in the different trends followed

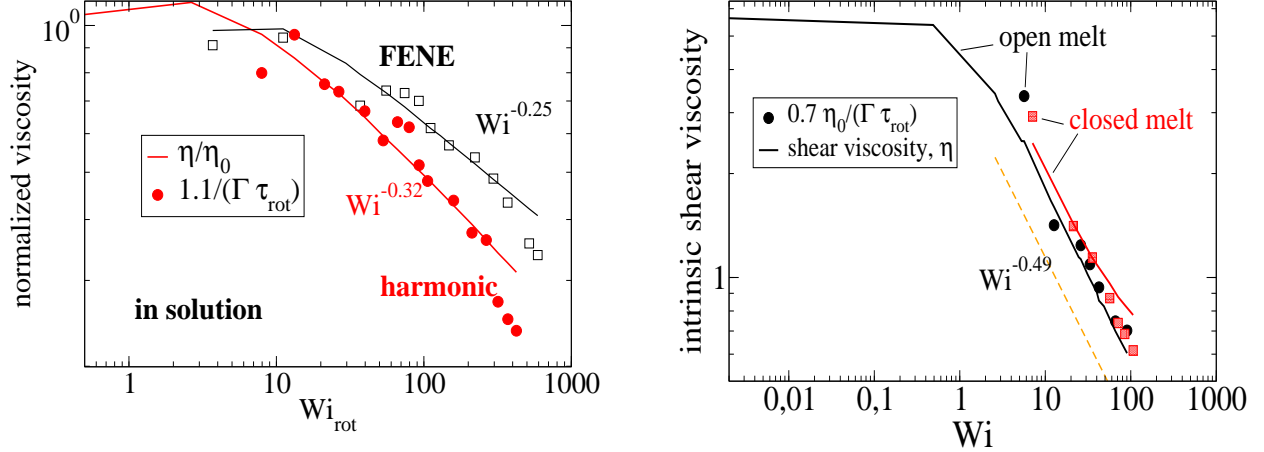


FIG. 7. The intrinsic shear viscosity η is compared with the normalized decorrelation rate of the arms (center-to-end) distance $\Gamma\tau_{rot}$. The left panel corresponds to stars in dilute solution (here, we normalize with the viscosity at zero shear rate η_0) and the right panel to stars in melt (polymer volume fraction 0.2). In solution, the shear stress scales like $\sigma_{12} = c\dot{\gamma}/\Gamma$ with $c = 15$ for harmonic and $c = 7$ for FENE bonds.

by T_u and Γ in melts: unlike what it is observed in solution, T_u and Γ do not correlate (see Fig. 5 botom).

V. CONCLUSIONS

The main purpose of this work is to show that the Eckart formalism can be used to unveil the complex dynamics of soft molecules in flow. The application of the Eckart formalism to the dynamics of star molecules in shear flow permitted us to warn about the incorrect interpretation of the rotation dynamics of soft molecules (polymers) based on a standard (lab frame) analysis. In particular, the *apparent* angular velocity ω resulting from such analysis has not a clear dynamical interpretation (it is not the rotation frequency of the molecule). We have shown that the Eckart co-rotating frame correctly extracts the different types of motions in the rotating and vibrating molecule: pure rotation, vibration with no-angular momentum and vibrational angular momentum. Star molecules in shear flow perform a tank-treading motion¹¹ whereby monomers rotate around the center of the molecule, but for a given fixed shear rate, the molecule keeps a *roughly fixed* ellipsoidal overall shape (more precisely, they do not tumble). At large shear rates, the molecule performs another collective motion, which we called “breathing mode”¹⁹, whereby the gyration tensor of the molecule oscillates in time with a characteristic frequency Ω_B . We have

shown that each of these dynamics is associated with a different type of displacement in the Eckart frame. The pure rotational component of the Eckart frame, with a frequency Ω , describes the tank-treading frequency of the star ω_R . By extracting the thermal (incoherent) part of the kinetic energy of vibrations without angular momentum component, we find that the kinetic energy of the breathing mode coincides with the energy of “breathing” vibrations. Finally, in solution, we find that the decorrelation of the end-to-end arm distance, driven by Brownian diffusion at a rate Γ , correlates with the kinetic energy associated to vibrations (or more properly, fluctuations) with angular momentum, T_u . In melt, such correlation is not observed, and it seems that the energy $|T_u|$ of molecular deformations is mainly determined by intermolecular collisions (and thus density dominated).

In this work, we just consider star polymers with $f = 12$ arms and $m = 6$ monomers per arm. According to a recent analysis⁵⁸, star molecules become chain-alike for $f < 6$ so our stars are within the “colloidal-alike” regime. But, what would be the dynamics of more massive stars? While this question is open to future works, we have good reasons to believe that they will be quite similar to that found for $f = 12, m = 6$. In fact, several computational works for star polymers in dilute¹¹ and semidilute¹⁶ conditions, covered a relative large range of values of $f \leq 50$ and $m < 50$ and (by defining the proper Weissenberg number) they found that all data for ω collapse in a master curve, indicating that the length of the arms or the functionality was not essentially changing the polymer dynamics. The dynamics would surely change in case of a semidilute solution (or melt) if the stars have *very* long arms ($m > 100$), because entanglements should play a mayor role in distorting their rotation dynamics. However, we emphasize that the Eckart framework would be still applicable in such regime and provide valuable dynamic information.

It also has to be noted that the present analysis can be complementary to the more detailed normal mode analysis of vibrations, within the framework of the theory of molecular vibrations²⁹. In the latter, each internally rotating part of the molecule would require the introduction of additional internal coordinate systems inside the translating and rotating Eckart frame^{34–37,59–63}. Presently, we leave this discussion for the future work, since the main aim of this paper is the separation of rotations from vibrations, or the consequences such decomposition brings up in the interpretation of molecular rotations. The objective of this work is to show that the Eckart frame, successfully and routinely used to describe Raman spectra of small molecules, is also a robust and useful tool to investigate the complex dynamics of soft, semiflexible macromolecules.

APPENDIX: THE ECKART REFERENCE CONFIGURATION

In the Eckart frame formalism of Eqs. 14 and 15, one needs to define a reference configuration which fixes c_i^α over time. These are the components of the monomers positions of the reference configuration in the initial internal coordinate system. We choose c_i^α in three different ways: **(i)** From an equilibrium configuration of a star polymer at temperature 0 K. **(ii)** The reference configuration is obtained by Metropolis Monte Carlo (MC) simulation at the desired temperature $T = 4$, which enforces by additional terms in the Hamiltonian that the configuration matches the average gyration tensor components at every shear rate. **(iii)** The c_i^α s are not constant. Instead, they are changed after a certain number of sampled configurations in the trajectory. An instantaneous configuration is taken as a reference configuration for the following τ_w in time, i.e. this configuration is used to evaluate the angular velocity of rotation (using the Eckart frame formalism) from all the following trajectory snapshots within the time window τ_w . Next, the first configuration following in the trajectory is taken as the new reference configuration. This procedure is thus repeated from the start until the end of the sampled trajectory. We analyze the rotation of molecules for different lengths of the time window and thus give the result for this third characterization of rotation by the Eckart frame formalism in the form of 3-dimensional plots (Fig. 8).

In all three described definitions of c_i^α s, the unit base vectors of the internal coordinate system \mathbf{f}_1 , \mathbf{f}_2 , and \mathbf{f}_3 and the origin of the Eckart frame, defined by \mathbf{r}_{cm} , are different in every snapshot of the sampled trajectory. Only the reference components c_i^α s remain constant throughout the whole trajectory in **(i)** and **(ii)**, while in **(iii)** also c_i^α s change in time, as described above. Molecules rotate in a flow-gradient plane. Therefore, the only component of the molecules' angular velocity with non zero-average is in the neutral direction and we denote, $\boldsymbol{\omega} = (\omega_1, \omega_2, \omega_3)$ and $\boldsymbol{\Omega} = (\Omega_1, \Omega_2, \Omega_3)$, where indices 1, 2, and 3 denote the flow, gradient, and neutral direction, respectively.

To determine the optimal way to define c_i^α s, we plot, in Fig. 8, angular velocities obtained by the Eckart formalism using the definitions **(i)**, **(ii)**, and **(iii)** for solution of star polymers with 12 arms of 6 monomers (connected by Hookean springs). Plots for the melt are qualitatively similar and are not shown here. We observe that the approach **(iii)**, in which c_i^α s change every τ_w , gives the angular velocity surface that at the shortest τ_w corresponds to the standard approach (i.e. using Eqs. 2 and 3). With increasing τ_w , it approaches the values obtained by the approaches **(i)** and **(ii)**. At a certain value of τ_w , we observe a sharp crossover in angular velocity of polymers at very high shear rates, which results in qualitatively different dependencies $\Omega/\dot{\gamma}(W_i)$ emerging only due to

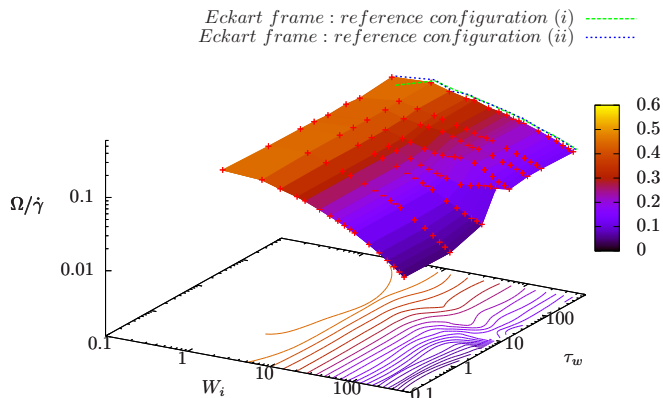


FIG. 8. Three definitions of reference configuration to calculate the angular velocity by Eckart frame formalism for star polymers in solution: **(i)** The reference configuration is the equilibrium configuration at temperature 0 K (green line). **(ii)** We obtain the reference configuration at every shear rate separately by the Monte Carlo simulation so that it matches the average steady state shape of a polymer (i.e. gyration tensor) at that particular shear rate (blue line). **(iii)** The reference configuration is taken to be an instantaneous one, but in this way defined c_i^α s are used in computation of the angular velocity only for the following τ_w in time. Afterwards, the reference configuration is replaced with the next instantaneous configuration, from which we define new c_i^α s.

the different reference frames. A similar crossover is also observed in melts, but is more prominent in solutions. Furthermore, we observe that this crossover occurs at higher τ_w for the star polymers with longer arms.

Importantly, we find that the definitions **(i)** and **(ii)** yield basically the same results, which are also similar to the results obtained by the definition **(iii)** after the crossover. Therefore, in the manuscript, we present only results obtained by the definition **(ii)**.

ACKNOWLEDGMENTS

J. S. and M. P. acknowledge financial support through grants P1-0002 and J1-7435 from the Slovenian Research Agency. J. S. acknowledges financial support from Slovene Human Resources Development and Scholarship Fund (186. JR). R. D.-B. acknowledges support from the Spanish government under national MINECO project FIS2013-47350-C5-1-R. Partial support from COST Action MP1305 is kindly acknowledged.

REFERENCES

- ¹D. E. Smith, H. P. Babcock, and S. Chu, *Science* **283**, 1724 (1999).
- ²R. E. Teixeira, H. P. Babcock, E. S. G. Shaqfeh, and S. Chu, *Macromolecules* **38**, 581 (2005).
- ³C.-C. Huang, G. Sutmann, G. Gompper, and R. G. Winkler, *Europhys. Lett.* **93**, 54004 (2011).
- ⁴S. Costanzo, Q. Huang, G. Ianniruberto, G. Marrucci, O. Hassager, and D. Vlassopoulos, *Macromolecules* **49**, 3925 (2016).
- ⁵R. G. Winkler, *Soft Matter* **12**, 3737 (2016).
- ⁶W. Chen, K. Zhang, L. Liu, J. Chen, Y. Li, and L. An, *Macromolecules* **50**, 1236 (2017).
- ⁷M. Abkarian, M. Faivre, and A. Viallat, *Phys. Rev. Lett.* **98**, 188302 (2007).
- ⁸A. Z. K. Yazdani and P. Bagchi, *Phys. Rev. E* **84**, 026314 (2011).
- ⁹W. R. Dodson and P. Dimitrakopoulos, *Biophys. J.* **99**, 2906 (2010).
- ¹⁰C. Aust, S. Hess, and M. Kröger, *Macromolecules* **35**, 8621 (2002).
- ¹¹M. Ripoll, R. G. Winkler, and G. Gompper, *Phys. Rev. Lett.* **96**, 188302 (2006).
- ¹²M. Ripoll, R. Winkler, and G. Gompper, *Eur. Phys. J. E* **23**, 349 (2007).
- ¹³Z.-C. Yan, S. Costanzo, Y. Jeong, T. Chang, and D. Vlassopoulos, *Macromolecules* **49**, 1444 (2016).
- ¹⁴K.-W. Hsiao, C. M. Schroeder, and C. E. Sing, *Macromolecules* **49**, 1961 (2016).
- ¹⁵J. Yoon, J. Kim, and C. Baig, *J. Rheol.* **60**, 673 (2016).
- ¹⁶W. Chen, J. Chen, and L. An, *Soft Matter* **9**, 4312 (2013).
- ¹⁷W. Chen, H. Zhao, L. Liu, J. Chen, Y. Li, and L. An, *Soft Matter* **11**, 5265 (2015).
- ¹⁸W. Chen, Y. Li, H. Zhao, L. Liu, J. Chen, and L. An, *Polymer* **64**, 93 (2015).
- ¹⁹J. Sablić, M. Praprotnik, and R. Delgado-Buscalioni, *Soft Matter* (2017, DOI: 10.1039/C7SM00364A), 10.1039/C7SM00364A, DOI: 10.1039/C7SM00364A.
- ²⁰A. Jain, C. Sasmal, R. Hartkamp, B. Todd, and J. R. Prakash, *Chem. Eng. Sci.* **121**, 245 (2015), 2013 Danckwerts Special Issue on Molecular Modelling in Chemical Engineering.
- ²¹R. Cerf, *J. Chim. Phys.* **68**, 479 (1969).
- ²²S. P. Singh, D. A. Fedosov, A. Chatterji, R. G. Winkler, and G. Gompper, *J. Phys.-Condens. Mat.* **24**, 464103 (2012).
- ²³S. P. Singh, A. Chatterji, G. Gompper, and R. G. Winkler, *Macromolecules* **46**, 8026 (2013).
- ²⁴T. Yamamoto and N. Masaoka, *Rheologica Acta* **54**, 139 (2015).

- ²⁵X. Xu and J. Chen, *J. Chem. Phys.* **144**, 244905 (2016).
- ²⁶R. Delgado-Buscalioni, J. Sablić, and M. Praprotnik, *Eur. Phys. J. Special Topics* **224**, 2331 (2015).
- ²⁷J. Sablić, M. Praprotnik, and R. Delgado-Buscalioni, *Soft Matter* **12**, 2416 (2016).
- ²⁸G. De Fabritiis, R. Delgado-Buscalioni, and P. Coveney, *Phys. Rev. Lett* **97**, 134501 (2006).
- ²⁹C. Eckart, *Phys. Rev.* **47**, 552 (1935).
- ³⁰E. Wilson, J. Decius, and P. Cross, *Molecular Vibrations: The Theory of Infrared and Raman Vibrational Spectra*, Dover Books on Chemistry Series (Dover Publications, 1955).
- ³¹J. D. Louck and H. W. Galbraith, *Rev. Mod. Phys.* **48**, 69 (1976).
- ³²Y. M. Rhee and M. S. Kim, *J. Chem. Phys.* **107**, 1394 (1997).
- ³³T. Yanao and K. Takatsuka, *J. Chem. Phys.* **120**, 8924 (2004).
- ³⁴D. Janežič, M. Praprotnik, and F. Merzel, *J. Chem. Phys.* **122**, 174101 (2005).
- ³⁵M. Praprotnik and D. Janežič, *J. Chem. Inf. Model.* **45**, 1571 (2005).
- ³⁶M. Praprotnik and D. Janežič, *J. Chem. Phys.* **122**, 174102 (2005).
- ³⁷M. Praprotnik and D. Janežič, *J. Chem. Phys.* **122**, 174103 (2005).
- ³⁸C. N. Likos, H. Löwen, M. Watzlawek, B. Abbas, O. Jucknischke, J. Allgaier, and D. Richter, *Phys. Rev. Lett.* **80**, 4450 (1998).
- ³⁹C. N. Likos, *Phys. Rep.* **348**, 267 (2001).
- ⁴⁰G. S. Grest, L. J. Fetters, J. S. Huang, and D. Richter, “Star polymers: Experiment, theory, and simulation,” in *Advances in Chemical Physics* (John Wiley and Sons, Inc., 2007) pp. 67–163.
- ⁴¹C. Hijon, P. Español, E. Vanden-Eijnden, and R. Delgado-Buscalioni, *Faraday Discuss.* **144**, 301 (2010).
- ⁴²A. A. Veldhorst, J. C. Dyre, and T. B. Schrøder, *J. Chem. Phys.* **143**, 194503 (2015).
- ⁴³P. Español and P. Warren, *Europhys. Lett.* **30**, 191 (1995).
- ⁴⁴T. Soddemann, B. Dünweg, and K. Kremer, *Phys. Rev. E* **68**, 046702 (2003).
- ⁴⁵A. W. Lees and S. F. Edwards, *J. Phys. C Solid State* **5**, 1921 (1972).
- ⁴⁶D. J. Evans and G. P. Morriss, *Phys. Rev. A* **30**, 1528 (1984).
- ⁴⁷A. J. Ladd, *Mol. Phys.* **53**, 459 (1984).
- ⁴⁸R. Delgado-Buscalioni, in *In Numerical Analysis of Multiscale Computations*, edited by Y.-H. R. T. Björn Engquist, Olof Runborg (Springer, 2011).
- ⁴⁹E. G. Flekkoy, R. Delgado-Buscalioni, and P. V. Coveney, *Phys. Rev. E* **72**, 026703 (2005).
- ⁵⁰M. Tuckerman, *Statistical Mechanics: Theory and Molecular Simulation*, Oxford Graduate

Texts (OUP Oxford, 2010).

- ⁵¹R. M. Jendrejack, M. D. Graham, and J. J. de Pablo, *J. Chem. Phys.* **113**, 2894 (2000).
- ⁵²R. M. Jendrejack, J. J. de Pablo, and M. D. Graham, *J. Chem. Phys.* **116**, 7752 (2002).
- ⁵³F. B. Usabiaga and R. Delgado-Buscalioni, *Macromol. Theor. Simul.* **20**, 466 (2011).
- ⁵⁴P. S. Doyle and P. T. Underhill, “Brownian dynamics simulations of polymers and soft matter,” in *Handbook of Materials Modeling: Methods*, edited by S. Yip (Springer Netherlands, Dordrecht, 2005) pp. 2619–2630.
- ⁵⁵K. Yasuda, *J. Text. Eng.* **52**, 171 (2006).
- ⁵⁶J. Aho, *Rheological Characterization of Polymer Melts in Shear and Extension: Measurement Reliability and Data for Practical Processing* (Tampere University of Technology, 2011).
- ⁵⁷M. Doi and S. F. Edwards, *The Theory of Polymer Dynamics* (Clarendon Press - Oxford, 1994).
- ⁵⁸A. Chremos and J. F. Douglas, *J. Chem. Phys.* **143**, 111104 (2015).
- ⁵⁹J. B. Howard, *J. Chem. Phys.* **5**, 442 (1937).
- ⁶⁰J. B. Howard, *J. Chem. Phys.* **5**, 451 (1937).
- ⁶¹B. Kirtman, *J. Chem. Phys.* **37**, 2516 (1962).
- ⁶²B. Kirtman, *J. Chem. Phys.* **41**, 775 (1964).
- ⁶³B. Kirtman, *J. Chem. Phys.* **49**, 2257 (1968).